In-situ strengthening of a high strength low alloy steel during Wire and Arc Additive Manufacturing (WAAM)

Tiago A.Rodrigues [1], V. Duarte [1], D. Tomás [1], Julian A. Avila [2], J. D. Escobar [3], Emma Rossinyol [4], N. Schell [5], Telmo G. Santos[1], J. P. Oliveira [1, *]

[1] UNIDEMI, Departamento de Engenharia Mecânica e Industrial, Faculdade de Ciências e Tecnologia, Universidade NOVA de Lisboa, Caparica, Portugal

[2] São Paulo State University (UNESP), Campus of São João da Boa Vista, Av. Profª Isette Corrêa Fontão, 505, Jardim das Flores, 13876-750, São João da Boa Vista, SP, Brazil

[3] Metallurgical and Materials Engineering Department, University of São Paulo, Av.Prof. Mello Moraes 2463, 05508-030, São Paulo, SP, Brazil

[4] Servei de Microscòpia, Universitat Autònoma de Barcelona, E-08193 Bellaterra, Spain

[5] Helmholtz-Zentrum Geesthacht, Institute of Materials Research, Max-Planck-Str. 1, Geesthacht, 21502, Germany.

* corresponding author: jp.oliveira@fct.unl.pt

Abstract

In this work, SiC particles were added to the molten pool during WAAM of a high strength low alloy steel. The introduction of these high melting point particles promoted grain refinement, and the precipitation of Fe_3C due to SiC dissociation. The microstructural evolution was studied by optical and electron microscopy techniques and high energy synchrotron X-ray diffraction. Additionally, mechanical testing and hardness profiles were obtained for the SiC-containing and SiC-free parts. An improvement in the mechanical strength of the SiC-added WAAM parts was observed, which was attributed to the refined grain structure and finely dispersed Fe_3C.

Keywords: Wire and Arc Additive Manufacturing; Inoculants; Synchrotron X-ray diffraction; mechanical testing; SiC; HSLA steel.

Graphical Abstract

In-situ strengthening of HSLA steel during Wire and Arc Additive Manufacturing
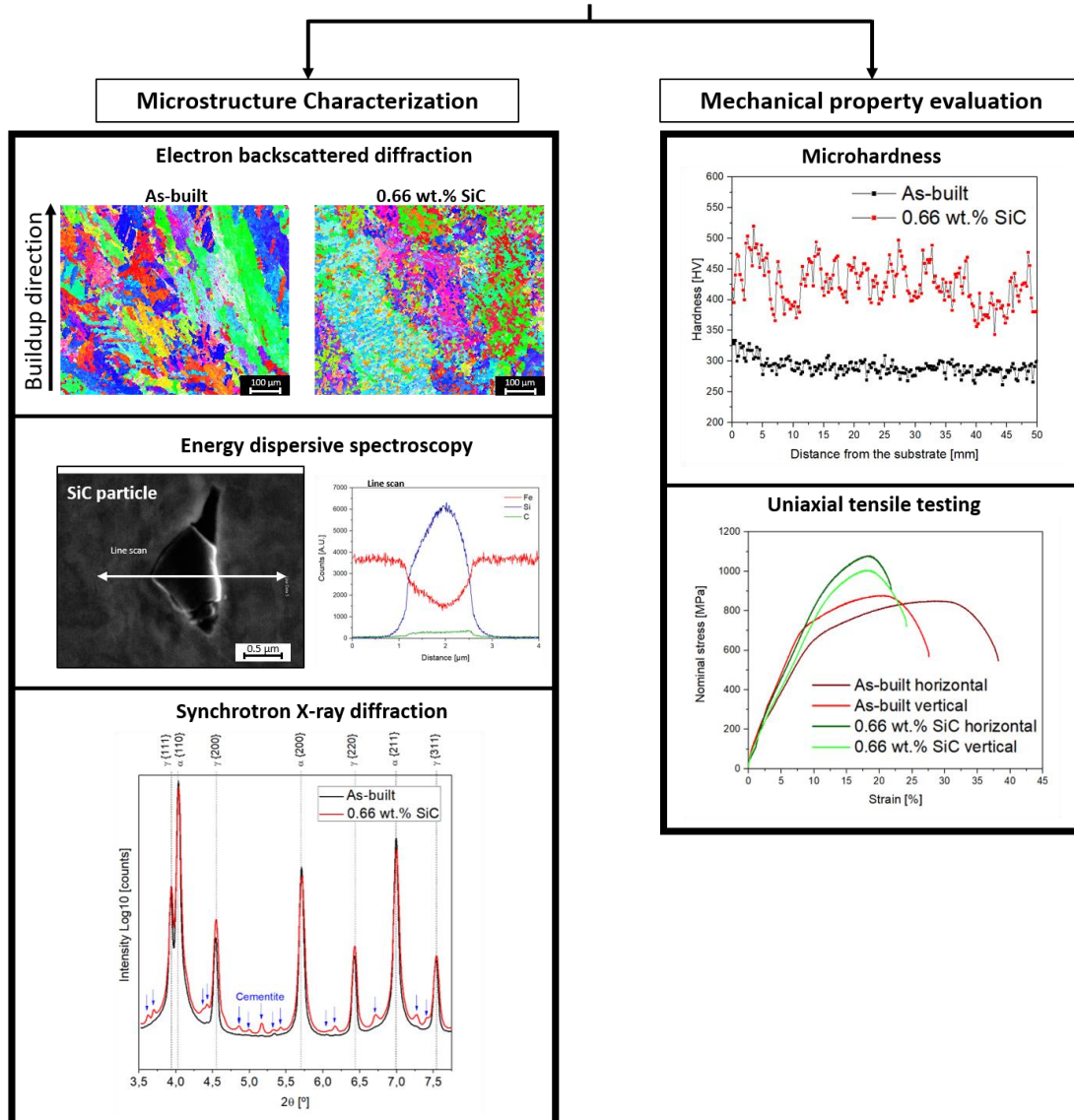
Highlights

- SiC particles were added in-situ during WAAM of an high strength low alloy steel.

- Cementite formed in the SiC-containing parts due to SiC dissociation in the melt pool.

- Non-melted SiC particles acted as nucleating agents promoting grain refinement

- Improved mechanical properties were obtained upon the use of SiC.

1. Introduction

Directed energy deposition techniques, in which focused thermal energy is used to melt the feedstock material, have enabled the production of large metallic components with medium complexity [1]. Among them, Wire and Arc Additive Manufacturing (WAAM) is being increasingly investigated, owing to several key characteristics, such as: large similarity with arc welding processes, where an extensive knowledge of the process parameters on different materials effects already exist; high deposition rates and material usage efficiency; and, finally, its ability to produce near-net-shape parts [2–4].

High strength low alloy (HSLA) steels are widely used for naval and automotive applications, as well as in the tools and die industries. WAAM of HSLA steels is reported in the literature [5,6]. It was inferred that the thermal cycles experienced during WAAM can influence the microstructure, thus influencing the local mechanical properties at different heights of the produced parts. One of the effects of extended periods at high temperatures during WAAM of HSLA steels is grain growth, resulting in a reduction in hardness. A potential solution to avoid material softening could involve increasing the time between consecutive deposited layers, which would reduce the amount of time spent at temperatures where grain growth occurs. However, the increase of dwell time between layers can be detrimental to the implementation of WAAM in a competitive industrial context.

One key strategy to counteract a decrease in hardness is to create HSLA WAAM parts with smaller grain sizes. This can be accomplished by reducing the heat input used to deposit the material or by using inoculants to change the nucleation and growth sequence during solidification. Inoculants can promote grain refinement, precipitation hardening, solid solution strengthening and even adjust the material composition [7]. Even though inoculation is a common practice in the metal casting industry, its use and effectiveness are yet to be explored in WAAM.

One potential inoculant is silicon carbide (SiC). Due to its high hardness (around 2500 HV), excellent corrosion resistance and high melting point, these ceramic particles have been proposed to be used during WAAM. For example, Meredy et al. [8] used SiC during the WAAM of a Titanium alloy. Its use was seen to refine the as-deposited prior-β grains. Yet, some columnar grains, typical of the WAAM process were still observed. Interestingly, the width of the columnar grains was reduced when SiC was used during deposition. This behavior was

3

attributed to the lateral rejection of Si-rich solute, which decreases the growth rate in the perpendicular direction to the heat flow extraction, resulting in narrower grains.

While the use of SiC or other inoculant particles is yet very limited in WAAM.SiC has already been used during selective laser melting to create a metal matrix composite. Song et al. [9] used sub-micron SiC powder (2.2 wt. %) with Fe to create Fe/SiC composites by selective laser melting. Partial dissolution of the particles occurred, which aided in the formation of martensite and pearlite. Some SiC particles were not fully melted and were found dispersed in the matrix. Additionally, mechanical testing showed that the yield strength increased with the use of SiC. In another study [10], laser surface alloying of SiC onto a mild steel substrate was performed. Even though multiple phases have been reported to form, it is believed that the increase in hardness and wear-resistance of the laser processed material can be attributed to the presence of cementite, formed as a consequence of the increased carbon content in solid solution due to the partial dissolution of SiC.

As it can be perceived, the inoculation of SiC particles during WAAM of steel could effectively improve the mechanical properties of the fabricated parts. In this study, the effect of the addition of SiC as inoculant particles during WAAM of an HSLA steel was assessed. Optical and scanning electron microscopy techniques were used to understand the microstructural modifications. High energy synchrotron X-ray diffraction was used to detail the secondary precipitation phenomena. Microhardness, mechanical and electrical conductivity testing were conducted to study the integrity of the deposited parts.

2. Experimental procedure

2.1 WAAM deposition

In this study, a customized WAAM machine was used. Previous work conducted by the authors, addressed the impact of different heat inputs on the thermal behavior, microstructural evolution and mechanical properties of a HSLA steel part produced by WAAM [5]. Those results will be used as a benchmark to evaluate the effect of SiC inoculation during WAAM. The wire feedstock material was a commercial HSLA steel wire electrode (ER110S-G) with a diameter of 1 mm, provided by *DRATEC*. The chemical composition of the wire is presented in Table 1.

Table 1 - Chemical composition of the ER110S-G wire electrode (wt.%).

C	Mn	Si	Ni	Cr	Mo	V	Cu	Fe
0.08	1.70	0.44	1.35	0.23	0.30	0.08	0.25	Balance

The HSLA steel was deposited onto a mild steel substrate using gas metal arc welding technique. A total of 50 layers were deposited, each one with a length of 180 mm. In between deposited layers SiC particles purchased from *GetNanoMaterials-GNM*, with a grain size ranging from 1 to 2 μm, were added. The particles were previously mixed in an ethanol gel solution and added via a customized feeding device depicted in Figure 1. The feeding device was placed 50 mm behind the molten pool, where the layer was at a temperature ranging between 200 and 300 ⁰C. This gel was selected due to its easy evaporation when in contact with the (still hot) already deposited layer. After the gel was evaporated, the SiC adhered to the deposited material and was incorporated into the molten pool when a subsequent layer was deposited. A concentration of 0.66 wt.% of SiC was used and its effect was compared to a non-modified (SiC-free) sample after WAAM.
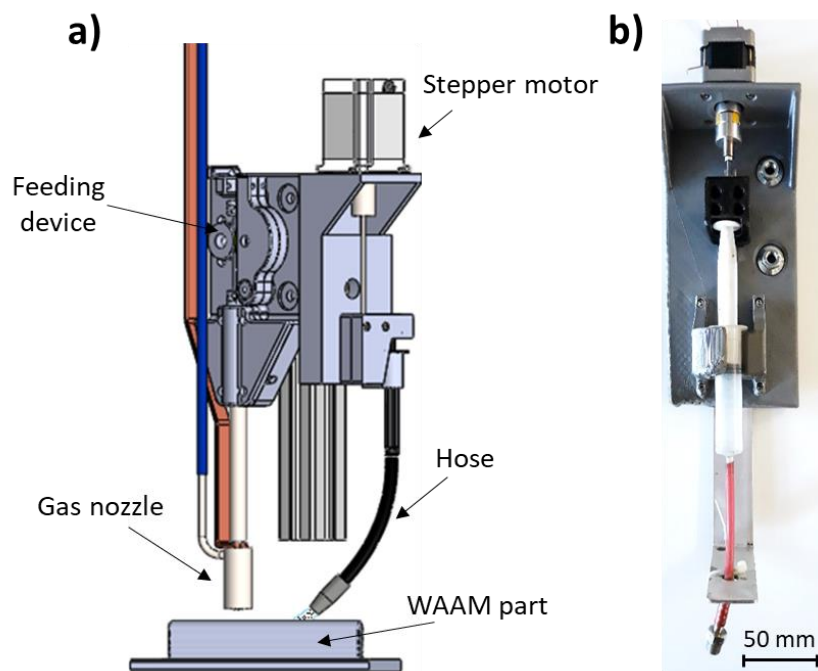

Figure 1 – Customized feeding device for in-situ inoculation during WAAM: a) schematic representation; b) actual device.

During deposition, the wire feed speed used was 3 m/min, while the travel speed was 5 mm/s. The welding equipment was set to a continuous wave mode with a voltage of 19 V, resulting in a heat input of 380 J/mm. The molten pool was protected with a flow rate of 16 L/min of

Alphagaz 1 (99.999% Ar). The deposition of a subsequent layer started after the temperature of the previous reached ≈ 100 °C.

2.2 Microstructural characterization

The microstructure of the produced samples was examined using a *Leica DMI 5000 M* inverted optical microscope. All samples were wire cut, polished, and etched with Nital (3%). Detailed microstructure analysis was performed using a Merlin scanning electron microscope (SEM) from Zeiss, while a Quanta 650 FEG SEM was used for electron backscattered diffraction (EBSD).

High energy synchrotron X-ray diffraction analysis was performed at the P07 7 High Energy Materials Science (HEMS) beamline at PETRA III, with a beam energy of 87.1 keV, corresponding to a wavelength of 0.1423 Å. Working in transmission mode, a 2D Perkin Elmer fast detector was used to capture the Debye-Scherrer diffraction rings. The obtained data was post processed using Fit2D software, as described in literature [11,12]. Analysis of the diffraction patterns, obtained from complete integration along the azimuthal angle, was conducted to evaluate fine microstructural details. For reference, the azimuthal angle,φ, is defined in Figure 2.
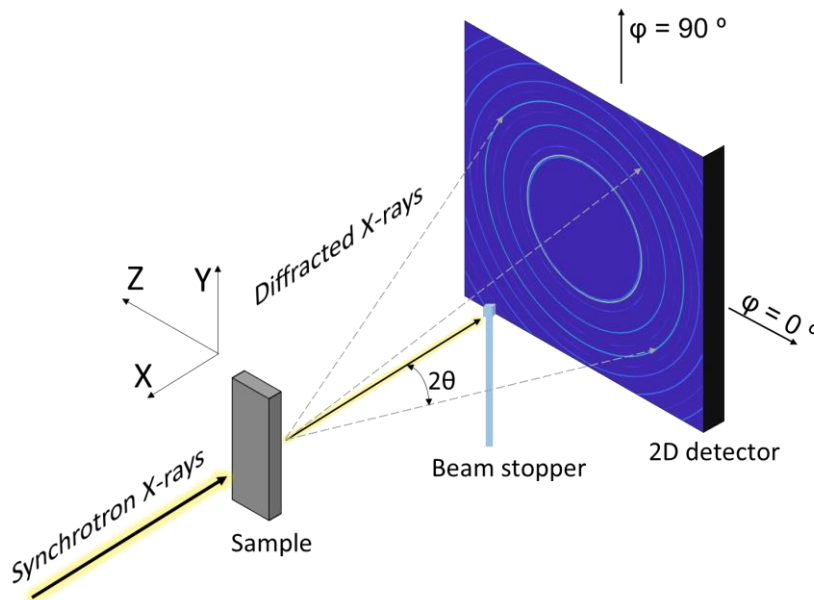

Figure 2 – Representation of the setup for the synchrotron X-ray diffraction experiments.

Peak fitting was performed to determine the influence of SiC addition on the material microstructure. The post processed 2D patterns were transformed, by full azimuthal

integration, into one dimensional intensity versus diffraction angle plots, and subjected to a peak fitting routine in order to extract information such as peak position, area and full width half maximum of the diffracted peaks. The quantification of retained austenite was performed following reference [13].

2.3 Microhardness and mechanical testing

Microhardness profiles along the height of the parts were performed using a Mitutoyo HM-112 Hardness Testing Machine, under a load of 1 kgf, with a holding time of 10 s. The distance between consecutive indentations was 250 μm. Uniaxial tensile tests were performed on a *MTS* hydraulic press with a capacity of 100 kN. The geometry of the samples used for uniaxial tensile testing is depicted in Figure 3. Five specimens were removed from both deposition (Y-axis), and build-up directions (Z-axis). The fracture surfaces were observed by SEM. A schematical representation of the extraction location of the samples used for each test is presented in Figure 4.
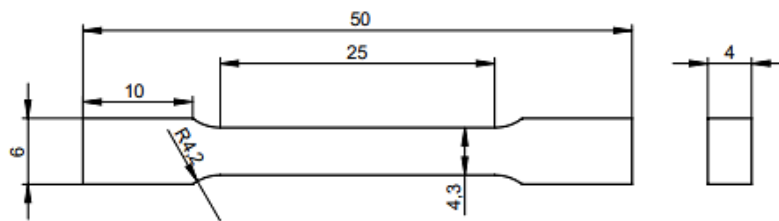

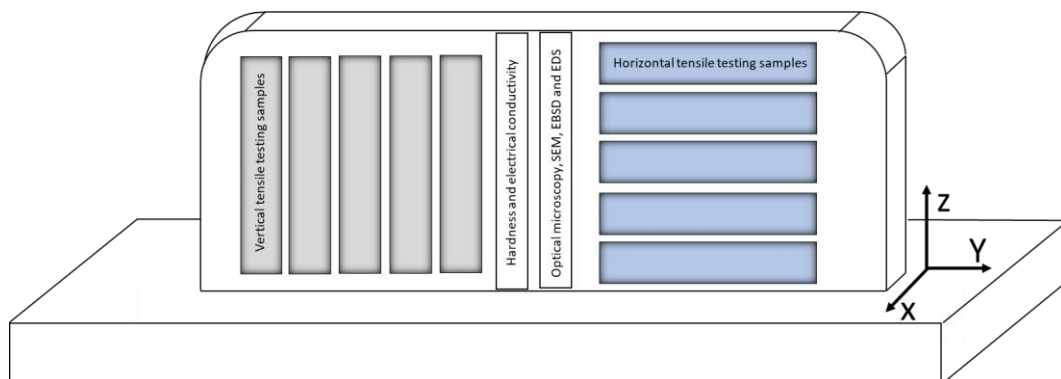*Figure 3 – Geometry and dimensions of the uniaxial tensile specimens.*

Figure 4 – Representation of the extraction location of the tested samples.

2.4 Electrical conductivity

To measure the changes in electrical conductivity between samples, a four-point potential drop technique was used. Measurements were made across the full height, starting in the substrate. The probe has a needle spacing of 635 μm, and a current of 80 mA was imposed

between the external needles. Electrical conductivity profiles can be used in thermomechanically processed materials to evaluate changes in composition, grain size, phase fraction and the existence of defects, as comprehensively evidenced in [14].

3. Results and discussion

3.1 Microscopic characterization

Figure 5 depicts optical macrographs of the produced samples. A significant difference in grain orientation and size is observed when comparing the samples with and without SiC. The non-inoculated sample exhibits coarse columnar grains aligned with the buildup direction (Figure 5 a). Whereas the SiC-containing sample has no discernible columnar grains (Figure 5 b).
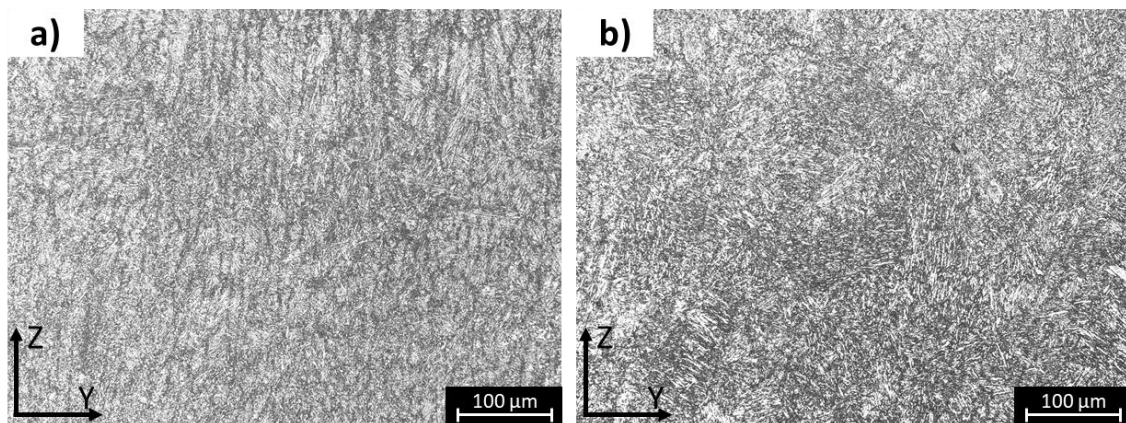

Figure 5 – Light optical macrographs of: a) HSLA with no SiC; b) HSLA with inoculation of 0.66 wt.% SiC.

Micrographs taken from the three orthogonal planes from both samples after WAAM are depicted in Figure 6. Columnar grains are visible in both YZ and XZ planes of the non-inoculated (as-built sample) sample, refer to Figure 6 a). In the XY plane, an equiaxed morphology is found, as this is a section view of the columnar grains. As for SiC-inoculated sample, a smaller grain structure, with diverse growth directions in the three orthogonal planes is observed (Figure 6 b).

According to Song, et al., the nucleation of ferrite on the previous austenite grain boundaries hinders the formation of massive columnar grains by growth restriction [9]. Additionally, the presence of unmelted particles can decrease the activation energy required for ferrite nucleation [15].

Through optical microscopy, only ferritic constituents can be observed in the matrix. The acicular morphology indicates the possible formation of bainite due to the accelerated cooling rate experienced during WAAM. The formation of bainite is expected to occur due to the fast cooling rate involved during solidification. The absence of pearlite and polygonal ferrite microstructures indicate that the cooling rate was faster than typical air cooling rates. On the other hand, the hardness values (discussed later in section 3.3) for the non-inoculated sample are lower than the expected martensitic hardness of around 350 HV for a carbon steel with around 0.1 wt% C [16]. Additionally, since the carbon content of the wire feedstock material is smaller than 0.2 wt.%, the impingement of allotriomorphs across austenite grains minimizes the possible growth of Widmanstatten ferrite. Hence, acicular ferrite is formed from the retained austenite with further cooling [7,15]. If there are no potent inclusions, bainitic ferrite might form instead of acicular ferrite, from the remaining austenite.

The bainitic microstructure is more notorious in the SiC inoculated sample. This is expected due to several competing phenomena, such as the increased carbon content from the dissociated SiC particles and the inoculation effect due to eased heterogeneous nucleation from small SiC inclusions and consequent grain grow in different directions [15]. However, from the authors previous work [5], it is known that martensite-austenite (M-A) islands and granular bainite constituents may appear. Though, its conclusive morphological identification is only possible via electron microscopy techniques using electron diffraction. These M-A constituents are produced from an incomplete transformation from austenite to martensite upon cooling, or after reheating to intercritical temperatures [19], with subsequent fast cooling rates, which occurs repetitively during WAAM.
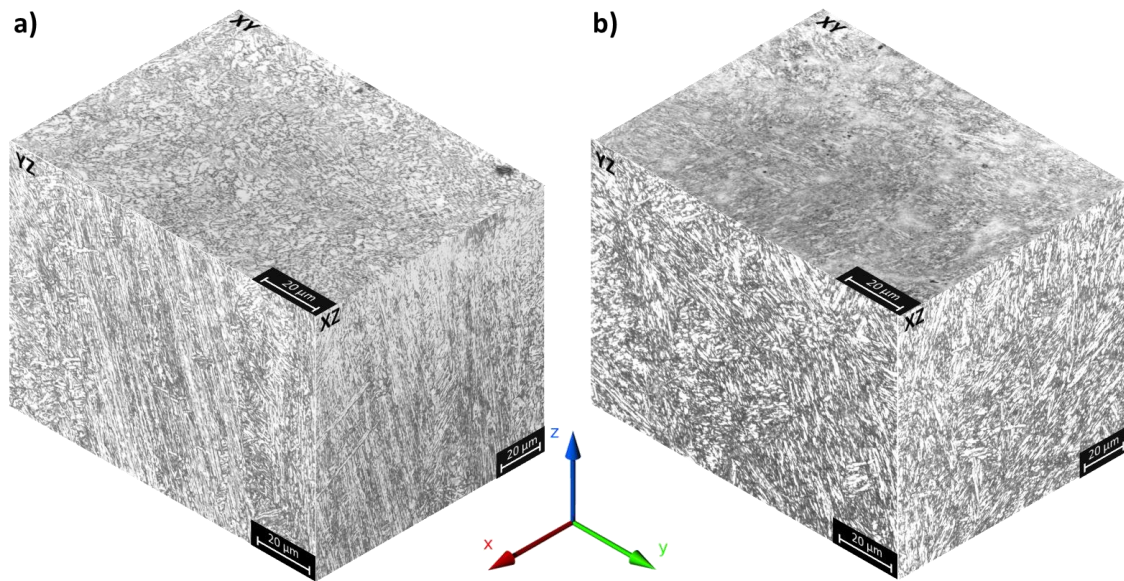
Figure 6 – Isometric micrographs of sample: a) HSLA as-built; b) HSLA with 0.66 wt.% SiC.

A more detailed analysis of the microstructure of the inoculated WAAM part is presented in the SEM image depicted in Figure 7. The existence of multiple phases including bainitic ferrite, M-A and cementite (Fe_3C) are observed. Also, some dispersed SiC particles are identified. The main difference in terms of existing phases compared to the non-inocullated sample (refer to [5]) is the existence of finely dispersed cementite and sparse SiC particles.
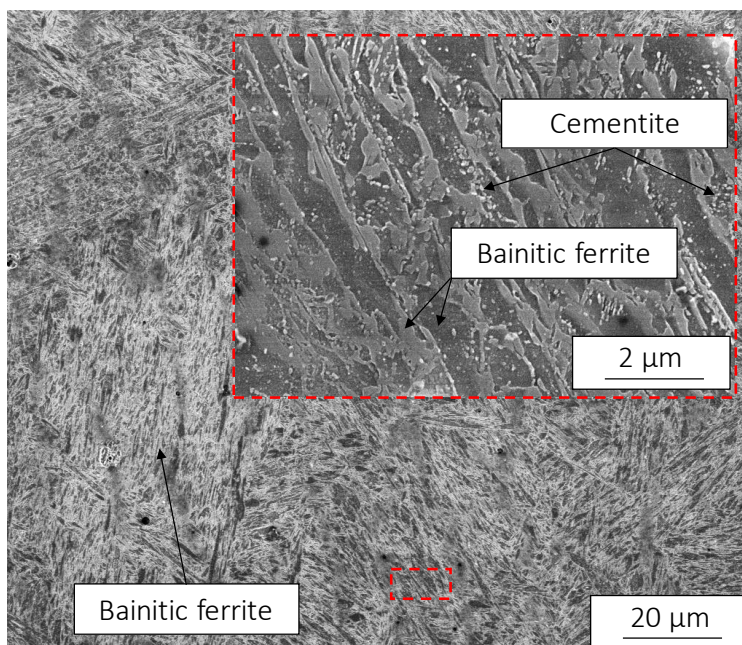

Figure 7 – Scanning electron microscopy image of the HSLA sample produced with SiC particles.

Figure 8 a) depicts a SEM micrograph of the non-inoculated WAAM part, revealing the presence of elongated columnar grains. Whereas, a refined grain structure is observed when

SiC particles are added during WAAM (Figure 8 b). These results are in good agreement with the previous light optical micrographs.
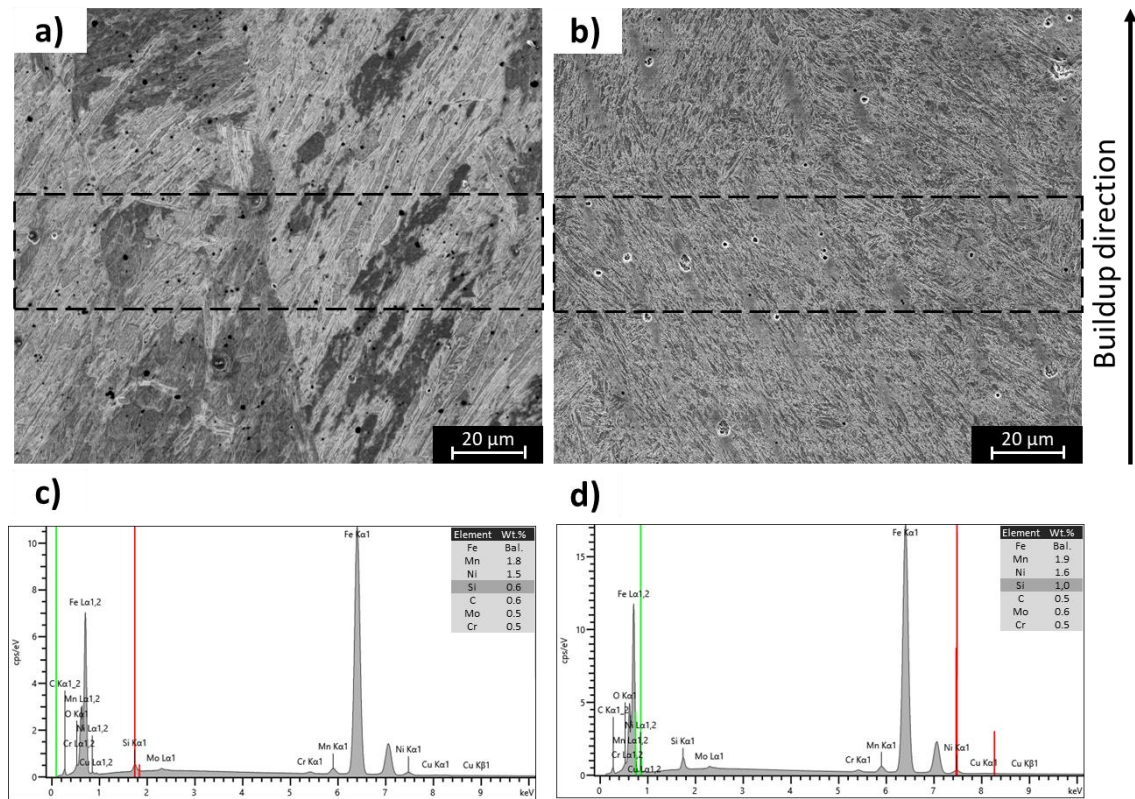

Figure 8 – Scanning electron microscopy images of samples: a) HSLA as-built; b) HSLA with 0.66 wt.% SiC; c) and d), energy dispersive spectra and chemical composition of the SiC-free and SiC-added WAAM parts, respectively. The dashed rectangles in a) and b) show the area that was used to determine the overall composition of the produced parts.

Energy-dispersive X-ray spectroscopy (EDS) was performed to evaluate the effect of introducing SiC particles during WAAM on part composition. The dashed boxes in Figure 8 a) and b) indicate the regions where compositional measurements were conducted. The semi-quantitative Si content in the non-inoculated sample (Figure 8 c) was found to match that of the electrode used (≈ 0.6 wt. %). For the SiC-containing sample, the Si content increased up to 1.0 wt. % (Figure 8 d). This increase indicates that the introduction of SiC into the melt pool was successful. However, during both optical and electron microscopy characterizations, the identification of the SiC particles was difficult, suggesting that strong or complete dissolution should have occurred during WAAM. Nevertheless, some dispersed SiC particles were found in the WAAM part matrix. Figure 9 depicts an example of one of those non-dissociated particles with an EDS line scan performed over it. The length of the particle (≈ 1.5 µm) is in good agreement with the original dimensions of the SiC particles used (ranging from 1 to 2 µm). As such, it can be inferred that the heat input was not enough to fully melt all the SiC particles.

Owing to the relatively low-value fraction of SiC particles determined by electron microscopy (< 1%), it can be stated that most of the inoculated particles were dissolved during the process. Note that some of the black dots observed in Figure 8 a) and b) are caused by local pitting during etching of the samples and not to residual SiC particles.
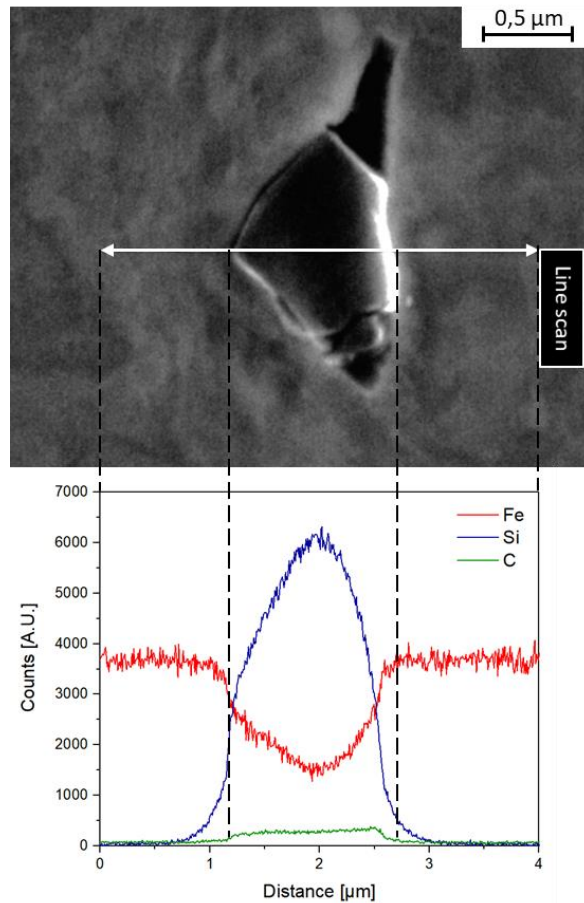

Figure 9 - Energy-dispersive X-ray spectroscopy line scan over a SiC particle in a WAAM sample inoculated with 0.66 wt.% of SiC.

The partial dissociation of the SiC particles in the melt pool can be attributed to their very high melting point (around 2800 °C), granulometric size, but also to their relative location to the heat source. If the particles are right below or near the heat source, the experienced peak temperature during the process will be higher and therefore melting of the SiC particles is more likely to occur. In opposition, if the particles are located towards the edges of the molten pool, the temperatures reached will be lower and complete dissolution can be hindered.

Electron backscattered diffraction (EBSD) analysis was performed for the non-inoculated and inoculated samples, and the results are shown in Figure 10 a) and b), respectively. When no SiC particles were used, columnar grains with a width of about 10 µm were observed. Contrasting,

the inoculated sample evidenceded refined grains with an average width size of 2.5 µm in the SiC-containing part. The EBSD results indicate the existence of an acicular microstructure with mostly bainite. However, the bainite packets are larger in the inoculated sample.
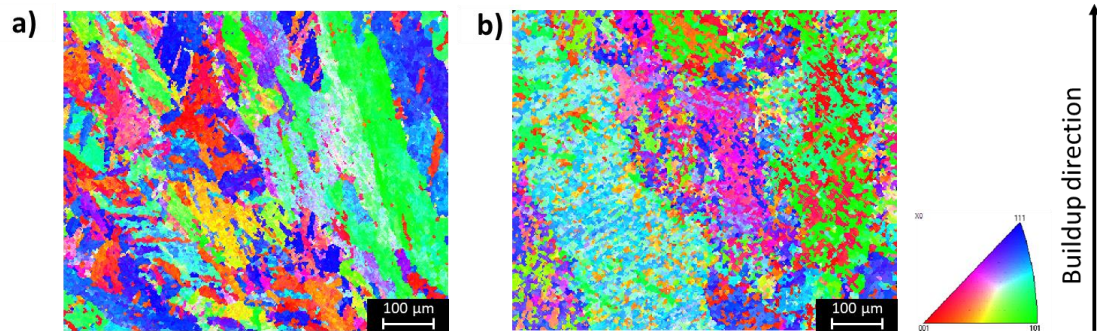

Figure 10 – Electron backscattered diffraction (EBSD) orientation maps of sample: a) HSLA as-built; b) HSLA with 0.66 wt.% SiC.

Analysis of the misorientation angles of the ferritic grains was performed (Figure 11). Both conditions exhibited a high content of low angle grain boundaries (< 15°). The frequency for misorientation angles between 15 and 50° is low, while it increases again for misorientation angles above 50°. The existence of boundaries with misorientation angles between 50 and 60° are related to upper and lower bainite [17] and fine bainite [20].
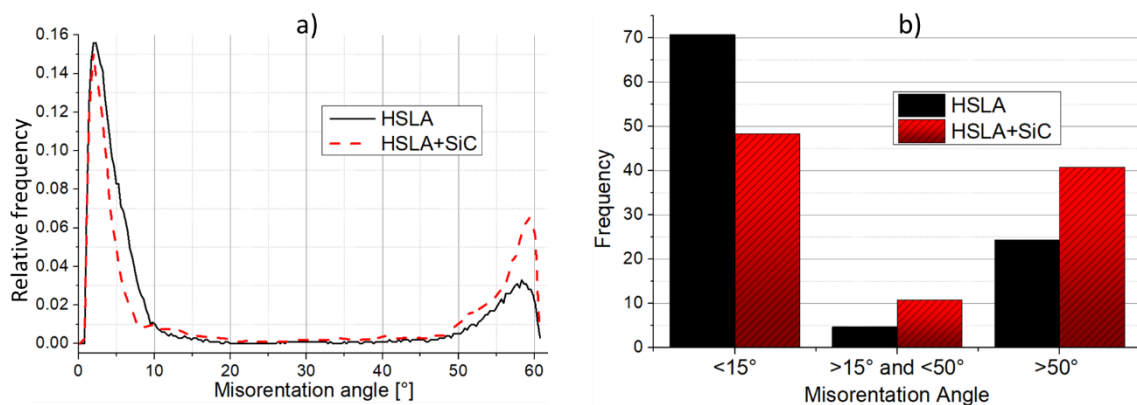

Figure 11 – Distribution of the misorientation angles of the ferritic grains in the as-built (HSLA) and inoculated (HSLA + SiC) WAAM parts: a) boundary distribution and b) frequency of low (< 15°) and high angle (> 15° and < 50°, and > 50°) boundaries.

3.2 Synchrotron X-ray diffraction results

Figure 12 depicts the high energy X-ray diffraction patterns of the two WAAM parts. Both exhibit retained austenite (γ) and ferrite (α) as the main volumetric phases.

The multi-peak fitting for the austenitic {111}, {200}, {220}, {311}; and ferritic {110}, {200} and {211} peaks evidenced the presence of retained austenite volume percentages of 12 and 18 % for the non-inoculated and inoculated samples, respectively. The increased presence of retained austenite (M-A) can be attributed to the increased carbon content incorporated to the welding pool and also to the retardant effect of Si for the precipitation of Fe_3C, favoring the formation of carbon-rich austenite [21].

Besides retained austenite, the most obvious difference between the two samples is the clear existence of cementite in the SiC-containing sample, indicated as blue arrows in Figure 12. The non-inoculated sample shows the presence of retained austenite with little or no presence of cementite. This indicates that the cooling rate was enough to prioritize the formation of a bainitic microstructure with no presence of cemenite, with a residual presence of retained austenite. On the other hand, a more complex microstructure developed in the inoculated sample. Besides bainite and retained austenite, cementite was also present. The formation of Fe_3C is favored when the parent phase is supersaturated in carbon [22]. This indicates that the nominal carbon content of the sample increased. Since the only variable changing during deposition was the addition of the SiC particles, it can be assumed that the bainite formation in the inoculated sample is accompanied by precipitation of cemenite.

No evidence of SiC diffraction peaks are found in X-ray diffraction patterns. This is related to the very low volume fraction of solid SiC particles found by scanning electron microscopy. Though synchrotron X-ray diffraction is able to detect small volume fraction phases [23–25], such was not possible in this case.
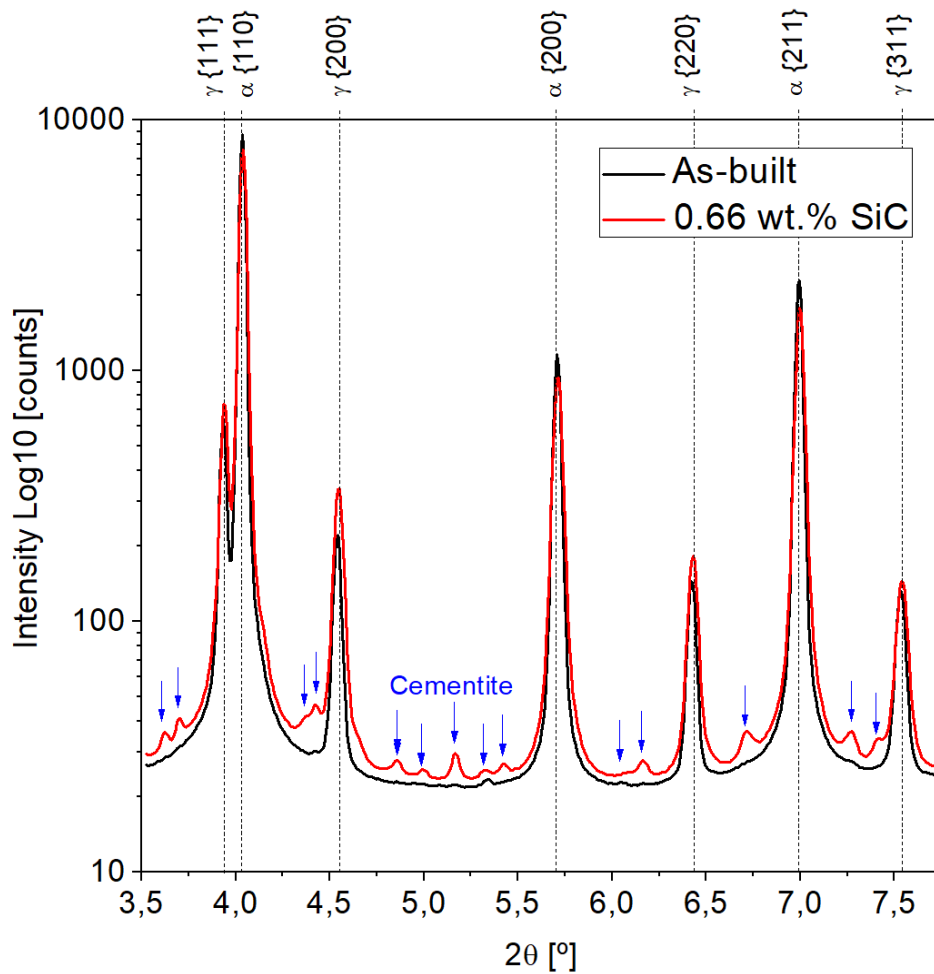
Figure 12 -Diffractogram of the sample: black) HSLA as-built; red) HSLA with 0.66 wt.% SiC. γ – austenite; α – ferrite.

Si is an alloying element known to suppress the precipitation of Fe_3C from austenite during the bainitic transformation. The addition of Si reduces the driving force for the formation of Fe_3C when this phase is forced to inherit the Si present in the parent phase [26–28]. Additionally, cementite growth is governed by Si partitioning. The rejected Si is piled up at the carbide-matrix interface, which decreases the flux of carbon from the matrix. This reduced carbon flux slows down the Fe_3C precipitation [29–31], causing the residual austenite to become carbon-enriched [31,32].

Research by Kozeschnik and Bhadeshia [22] indicates, that under equilibrium conditions, Fe_3C formation is hardly influenced by the Si content. In paraequilibrium conditions [33], i.e., the Fe/Si atom ratios are the same in the parent and growth phase, Fe_3C precipitation is retarded as the Si is trapped in the cementite. However, when the material is held at ≈ 300 °C, the partitioning of Si occurs, and Fe_3C precipitates. Previous work on WAAM of this HSLA steel [5]

showed that this temperature occurs multiple times in the already deposited layers due to the consecutive cycles of reheating experienced during sample build-up.

The effect of the SiC particles during the production of the HSLA steel parts was not solely observed on the solid-state transformation experienced by the material upon successive reheating cycles. It also impacted the grain morphology of the as-solidified material (refer to Figure 6). When SiC particles dissociated, Si-rich solute promotes constitutional supercooling, which has a refinement effect in HSLA steels [8]. It is recognized that constitutional supercooling plays an important role in promoting nucleation and grain formation [34]. During an alloy solidification, the driving force for nucleation is governed by the formation of constitutional supercooling, where segregation between the solid and liquid interface lowers the freezing range, which, in turn, reduced the growth rate of columnar grain structures [35].

As the amount of constitutional supercooling exceeds the supercooling necessary for nucleation, additional nucleation events occur in constitutionally supercooled zones. Constitutional supercooling can also protect the already formed-grains to be remelted when temperature fluctuations occur due to convection in front of growing grains. It must be noted that some factors can reduce the likelihood of constitutional supercooling to promote nucleation. These include the formation of a nucleation free zone [34] around each growing grain and solute accumulation between already growing grains. In this study, the increase of Si content in the molten pool was found to reduce the grain growth speed, and to promote more nucleation events, which ultimately resulted in smaller and more uniform grain size.

3.3 Mechanical properties

Tensile testing of the SiC and non-SiC WAAM parts was performed. The tensile curves of produced samples tested along different orientations (refer to Figure 4), is depicted in Figure 13. The elongation to fracture, yield and ultimate tensile strength of both parts, obtained along the vertical and horizontal directions are summarized in Table 2.
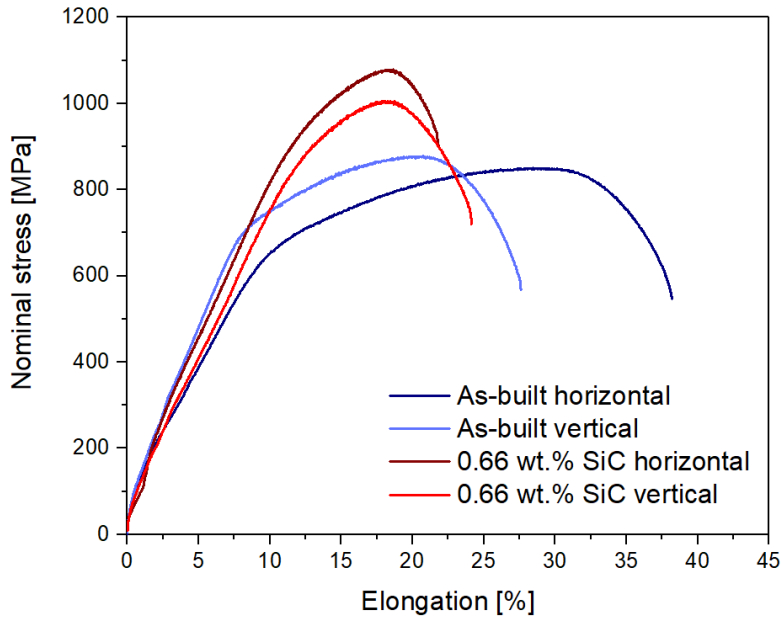
Figure 13 – Tensile curves of SiC and non-SiC WAAM parts tested along the horizontal and vertical directions.

Table 2 – Summary of mechanical properties of the SiC-free and SiC-containing HSLA steel parts obtained from uniaxial tensile testing

Sample Reference	Yield Strength [MPa]		Ultimate Tensile Strength [MPa]		Elongation to Fracture [%]	
	Horizontal	Vertical	Horizontal	Vertical	Horizontal	Vertical
As-built HSLA	681±25	707±33	870±37	889±16	39±2,1	30±2,8
HSLA/SiC	876±22	886±26	1070±25	1035±31	23±1,2	24±0,8

The introduction of the SiC particles and their massive dissociation during the WAAM process resulted in an increase of the yield strength by 195 and 179 MPa, in the horizontal and vertical directions, respectively. The ultimate tensile strength of the SiC containing samples increased by 200 MPa (23 %) and 146 MPa (16 %) in the horizontal and vertical directions when compared to the SiC-free specimens. Finally, the elongation to fracture of the inoculated samples was seen to decrease by 16 % and 6 %, with the addition of SiC.

Overall, there was a significant increase in the mechanical strength of the SiC-inoculated samples. However, this improvement came at the expense of reduced ductility. This effect can be attributed to the microstructural differences between both samples. The strengthening mechanisms that justifies the higher mechanical strength of the SiC-added parts include dislocation pinning due to the existence of more grain boundaries, and the fine dispersion of Fe_3C particles. Following the Hall-Petch relation [36,37], it is known that grain boundaries act

as pinning points, hindering dislocation movement under service conditions. A decrease in the grain size will increase the amount of required stress necessary for dislocations to move, thus, strengthening the material. Grain refinement of ferrite is one of the most common strengthening methods of steels [7]. Even though the volume fraction of austenite in the SiC containing sample was higher, the effect of ferrite grain size and Fe_3C precipitates prevails as another important factor (in combination with Fe_3C precipitation) regarding the improvement of the parts' mechanical strength.

Another strengthening mechanism for the inoculated samples is related to the differences in the thermal properties between Fe_3C and the sourrounding material matrix. The mismatch of the coefficient of thermal expansion between cementite and the surrounding matrix is high (4.1×10^{-5} vs 12×10^{-6} K). As such, the multiple heating and cooling steps due to consecutive depositions lead to the generation of dislocations [38]. This increased dislocation density also contributes to the increase in the mechanical strength of the parts. It should be noted that the elongation to fracture in both horizontal and vertical directions of the inoculated samples is similar, which is in good agreement with the microstructure characterization, suggesting a significant decrease of the anisotropy upon the introduction of SiC particles.

Fracture analysis of the tested samples (Figure 14) revealed the presence of dimples, in excellent agreement with the high plasticity of both the inoculated and non-inoculated parts.
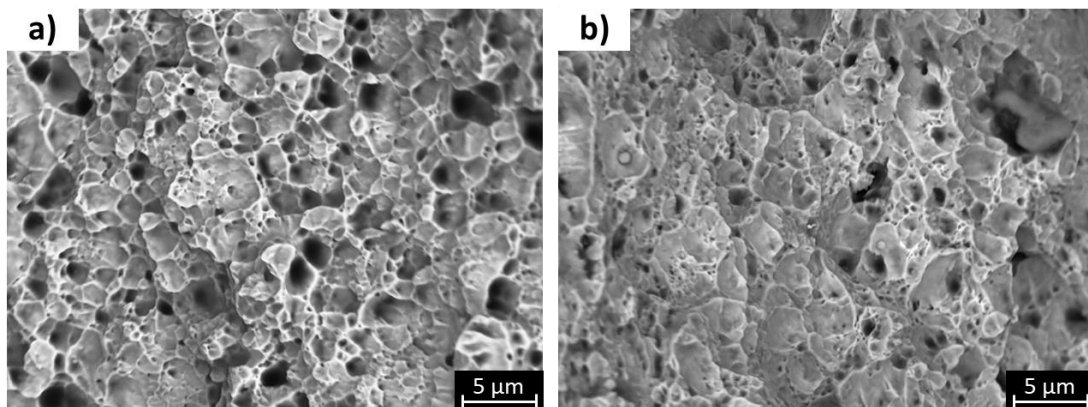

Figure 14 - Scanning electron microscopy image of a surface fracture of sample: a) HSLA as-built; b) HSLA with 0.66 wt.% SiC.

As HSLA steel can be used as structural parts, evaluation of the material hardness is also essential. The effect of SiC addition on the material hardness is depicted in Figure 15. The hardness of the SiC-free sample was of approximately 290 HV, whereas for the SiC-added part a massive increase to $\approx$ 425 HV was measured. This significant hardness increase is attributed

to the higher nominal carbon content, higher presence of retained austenite (M-A), more refined grain structure and to the presence of finely dispersed Fe3C. The hardness at the top of the non-inoculated sample was around 325 HV, which is higher than that at the bottom, due to the sequence of depositions causing a tempering effect. This is consistent with literature findings, since the softening of bainite has been reported to be moderated upon tempering [39], while these hardness values are not typical for martensite [16].

On the other hand, the hardness of the inoculated sample was higher than the expected martensite hardness (approximately 350 HV) for the nominal content of 0.1 wt.% C. Therefore, carbon dissociation towards the matrix must have occurred. Some oscillations in the hardness profile along the part height can be justified based on the subsequent interpass tempering sequence and the irregular distribution of SiC which can influence the location where Fe3C forms. Additionally, this increase in hardness is not expected to be due to the presence of the SiC particles in the matrix. The irregularity dispersion of particles in the inoculated samples can be attributed to the process itself, or by the fluid flow of the molten pool, which is governed by the liquid viscosity, temperature and concentration gradients, surface tension, Marangoni force and arc pressure [40].
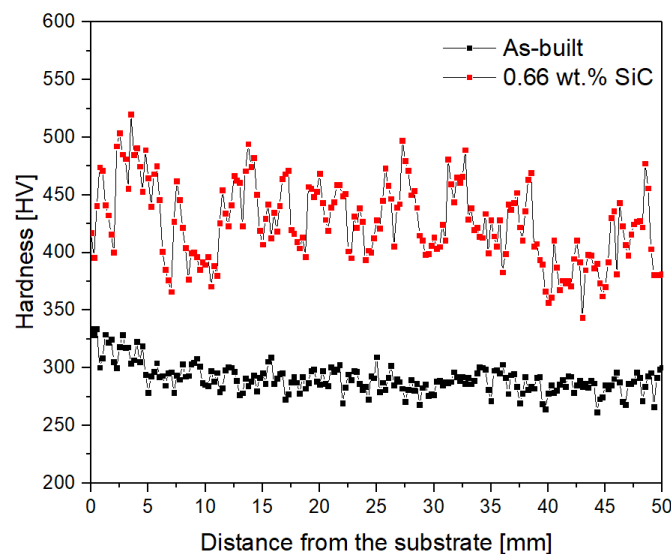

Figure 15 – Microhardness profiles of the non-inoculated (black) and 0.66 wt.% SiC inoculated (red) samples.

3.4 Electrical conductivity measurements

Electrical conductivity measurements along the samples height were also performed (Figure 16). Although electrical conductivity is sensitive to the chemical composition of the material,

the effect of grain size is predominant [41]. Variation in electrical conductivity, aside from allowing the detection of defects or discontinuities, enables the detection of microstructural features, such as grain refinement or coarsening, since more grain boundaries or precipitates hinder the electron movement.
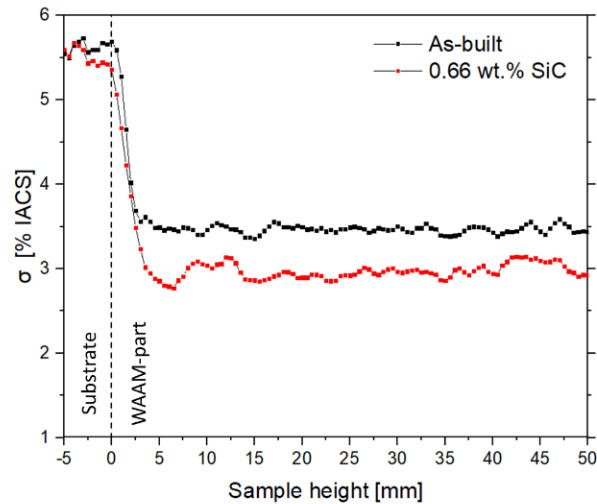

Figure 16 – Electrical conductivity measurements with a four-point probe.

The electrical conductivity profiles depicted in Figure 16 are in good agreement with the microstructure analysis. When the probe is moved from the substrate through the height of the sample, there is a sharp decrease in the electrical conductivity indicating the interface between the substrate and the first deposited layer. As the substrate used in this work is mild steel, its carbon content is higher than the wire feedstock used for the WAAM depositions, thus a higher conductivity is found in the substrate. Upon the introduction of the inoculants, the electrical conductivity of the inoculated part reduced from 3.5 to 3 % IACS. The existence of a refined grain structure of bainite and retained austenite with a high density of dislocations, and dispersed Fe_3C precipitates act as a barrier to the electron movement, resulting in a decrease of electrical conductivity. Of special interest is the inverse relationship between electrical conductivity and hardness: a lower electrical conductivity translates into a higher material hardness, and vice-versa. This correlation is in good agreement with existent literature on the topic [14].

4. Conclusions

In the present study, SiC particles were added *in-situ* during WAAM of a high strength low alloy steel. The main findings include:

- Microstructural observations revealed the presence of a more homogenous microstructure in the sample inoculated with SiC particles. Near isotropic grains formed upon the introduction of SiC into the molten pool.

- The dissociation of the SiC particles in the molten pool led to an increased carbon content in austenite, which resulted in the coexistence of bainite, retained austenite (M-A) and Fe_3C. The hardness increased, on average, from 290 up to 426 HV.

- Some SiC particles remained in the solid state during the WAAM process adding more nucleation sites upon solidification, resulting in a refined and more equiaxed solidification structure.

- The tensile strength of the SiC-inoculated samples was significantly improved compared to the non-inoculated ones. This increase is attributed to the refined grain structure, higher carbon content, retained austenite, and Fe_3C precipitation in the inoculated samples.

- Electrical conductivity measurements exhibit an inverse relation with the hardness profiles: an increase of hardness reflected the decrease in grain size and in electrical conductivity.

5. Acknowledgments

6. References

[1]   C.R. Cunningham, J.M. Flynn, A. Shokrani, V. Dhokia, S.T. Newman, Invited review article: Strategies and processes for high quality wire arc additive manufacturing, Addit. Manuf. 22 (2018) 672–686. doi:10.1016/j.addma.2018.06.020.

[2]   S.W. Williams, F. Martina, A.C. Addison, J. Ding, G. Pardal, P. Colegrove, Wire + Arc Additive Manufacturing, Mater. Sci. Technol. 32 (2016) 641–647. doi:10.1179/1743284715Y.0000000073.

[3]   T.A. Rodrigues, V. Duarte, R.M.M. Miranda, T.G. Santos, J.P.P. Oliveira, Current status and perspectives on wire and arc additive manufacturing (WAAM), Materials (Basel). 12 (2019) 1121. doi:10.3390/ma12071121.

[4]   J.P. Oliveira, T.G. Santos, R.M. Miranda, Revisiting fundamental welding concepts to improve additive manufacturing: From theory to practice, Prog. Mater. Sci. 107 (2019) 100590. doi:10.1016/j.pmatsci.2019.100590.

[5]   T.A. Rodrigues, V. Duarte, J.A. Avila, T.G. Santos, R.. Miranda, J.. Oliveira, Wire and arc additive manufacturing of HSLA steel: Effect of thermal cycles on microstructure and mechanical properties, Addit. Manuf. 27 (2019) 440–450. doi:10.1016/j.addma.2019.03.029.

[6]   P. Dirisu, S. Ganguly, A. Mehmanparast, F. Martina, S. Williams, Analysis of fracture toughness properties of wire + arc additive manufactured high strength low alloy structural steel components, Mater. Sci. Eng. A. 765 (2019) 138285. doi:10.1016/j.msea.2019.138285.

[7]   Harry Bhadeshia Robert Honeycombe, Steels: Microstructure and Properties, 3rd Editio, n.d.

[8]   S. Mereddy, M.J. Bermingham, D.H. StJohn, M.S. Dargusch, Grain refinement of wire arc additively manufactured titanium by the addition of silicon, J. Alloys Compd. 695 (2017) 2097–2103. doi:10.1016/j.jallcom.2016.11.049.

[9]   B. Song, S. Dong, P. Coddet, G. Zhou, S. Ouyang, H. Liao, C. Coddet, Microstructure and tensile behavior of hybrid nano-micro SiC reinforced iron matrix composites produced by selective laser melting, J. Alloys Compd. 579 (2013) 415–421. doi:10.1016/j.jallcom.2013.06.087.

[10]   G. Thawari, G. Sundarararjan, S. V. Joshi, Laser surface alloying of medium carbon steel with SiC(P), Thin Solid Films. 423 (2003) 41–53. doi:10.1016/S0040-6090(02)00974-4.

[11]   A.P. Hammersley, S.O. Svensson, M. Hanfland, A.N. Fitch, D. Hausermann, Two-dimensional detector software: From real detector to idealised image or two-theta scan, High Press. Res. 14 (1996) 235–248. doi:10.1080/08957959608201408.

[12]   J.P. Oliveira, F.M. Braz Fernandes, R.M. Miranda, N. Schell, J.L. Ocaña, Effect of laser welding parameters on the austenite and martensite phase fractions of NiTi, Mater. Charact. 119 (2016) 148–151. doi:10.1016/j.matchar.2016.08.001.

[13]   G.A. Faria, Exploring Metallic Materials Behavior Through In Situ Crystallographic Studies, (2014) 129.

[14]   G.L. Sorger, J.P.P. Oliveira, P.L. Inácio, N. Enzinger, P. Vilaça, R.M.M. Miranda, T.G. Santos, Non-destructive microstructural analysis by electrical conductivity: Comparison with hardness measurements in different materials, J. Mater. Sci. Technol. 35 (2019) 360–368. doi:10.1016/j.jmst.2018.09.047.

[15]   S.S. Babu, The mechanism of acicular ferrite in weld deposits, 8 (2004) 267–278. doi:10.1016/j.cossms.2004.10.001.

[16]   G. Krauss, Martensite in steel: strength and structure, Mater. Sci. Eng. A. 273–275 (1999) 40–57. doi:10.1016/S0921-5093(99)00288-9.

[17]   S. Zajac, V. Schwinnand, K.H. Tacke, Characterisation and quantification of complex bainitic microstructures in high and ultra-high strength linepipe steels, Mater. Sci. Forum. 500–501 (2005) 387–394. doi:10.4028/www.scientific.net/msf.500-501.387.

[18]   F.G. Caballero, M.K. Miller, C. Garcia-Mateo, Tracking solute atoms during bainite reaction in a nanocrystalline steel, Mater. Sci. Technol. (United Kingdom). 26 (2010) 889–898. doi:10.1179/026708310X12635619987943.

[19]   A. Lambert-Perlade, A.F. Gourgues, J. Besson, T. Sturel, A. Pineau, Mechanisms and

modeling of cleavage fracture in simulated heat-affected zone microstructures of a high-strength low alloy steel, Metall. Mater. Trans. A Phys. Metall. Mater. Sci. 35 (2004) 1039–1053. doi:10.1007/s11661-004-1007-6.

[20]   B. Hutchinson, J. Komenda, G.S. Rohrer, H. Beladi, Heat affected zone microstructures and their influence on toughness in two microalloyed HSLA steels, Acta Mater. 97 (2015) 380–391. doi:10.1016/j.actamat.2015.05.055.

[21]   M.H. Saleh, R. Priestner, Retained austenite in dual-phase silicon steels and its effect on mechanical properties, J. Mater. Process. Technol. 113 (2001) 587–593. doi:10.1016/S0924-0136(01)00638-0.

[22]   E. Kozeschnik, H.K.D.H. Bhadeshia, Influence of silicon on cementite precipitation in steels, Mater. Sci. Technol. 24 (2008) 343–347. doi:10.1179/174328408X275973.

[23]   J.P. Oliveira, A.J. Cavaleiro, N. Schell, A. Stark, R.M. Miranda, J.L. Ocana, F.M. Braz Fernandes, Effects of laser processing on the transformation characteristics of NiTi: A contribute to additive manufacturing, Scr. Mater. 152 (2018) 122–126. doi:10.1016/j.scriptamat.2018.04.024.

[24]   N. Jia, Z.H. Cong, X. Sun, S. Cheng, Z.H. Nie, Y. Ren, P.K. Liaw, Y.D. Wang, An in situ high-energy X-ray diffraction study of micromechanical behavior of multiple phases in advanced high-strength steels, Acta Mater. 57 (2009) 3965–3977. doi:10.1016/j.actamat.2009.05.002.

[25]   L.C.D. Fielding, N.G. Jones, J. Walsh, S. Van Boxel, M.S. Blackmur, P.D. Lee, P.J. Withers, H.J. Stone, H.K.D.H. Bhadeshia, Synchrotron analysis of toughness anomalies in nanostructured bainite, Acta Mater. 105 (2016) 52–58. doi:10.1016/j.actamat.2015.11.029.

[26]   D. Delagnes, P. Lamesle, M.H. Mathon, N. Mebarki, C. Levaillant, Influence of silicon content on the precipitation of secondary carbides and fatigue properties of a 5%Cr tempered martensitic steel, Mater. Sci. Eng. A. 394 (2005) 435–444. doi:10.1016/j.msea.2004.11.050.

[27]   W.J. Nam, H.C. Choi, Effect of Si on mechanical properties of low alloy steels, Mater. Sci. Technol. 15 (1999) 527–530. doi:10.1179/026708399101506238.

[28] G. Miyamoto, J.C. Oh, K. Hono, T. Furuhara, T. Maki, Effect of partitioning of Mn and Si on the growth kinetics of cementite in tempered Fe-0.6 mass% C martensite, Acta Mater. 55 (2007) 5027–5038. doi:10.1016/j.actamat.2007.05.023.

[29] J. Yu, Carbide stability diagrams in 2.25Cr-1Mo steels, Metall. Trans. A. 20 (1989) 1561–1564. doi:10.1007/BF02665512.

[30] B. Kim, C. Celada, D. San Martín, T. Sourmail, P.E.J. Rivera-Díaz-Del-Castillo, The effect of silicon on the nanoprecipitation of cementite, Acta Mater. 61 (2013) 6983–6992. doi:10.1016/j.actamat.2013.08.012.

[31] F.G. Caballero, H.K.D.H. Bhadeshia, Very strong bainite, Curr. Opin. Solid State Mater. Sci. 8 (2004) 251–257. doi:10.1016/j.cossms.2004.09.005.

[32] H. K. D. H. Bhadeshia, Bainite in steels: Transformations, Microstructure and Properties, 2nd ed., 2001.

[33] M. Hillert, J. Ågren, On the definitions of paraequilibrium and orthoequilibrium, Scr. Mater. 50 (2004) 697–699. doi:10.1016/j.scriptamat.2003.11.020.

[34] D.H. StJohn, A. Prasad, M.A. Easton, M. Qian, The Contribution of Constitutional Supercooling to Nucleation and Grain Formation, Metall. Mater. Trans. A Phys. Metall. Mater. Sci. 46 (2015) 4868–4885. doi:10.1007/s11661-015-2960-y.

[35] W. Kurz and D.J. Fisher, Fundamentals of Solidification, 3rd ed., Trans Tech Pubn, 1990.

[36] E.O. Hall, The deformation and ageing of mild steel: III Discussion of results, Proc. Phys. Soc. B. 64 (1951) 747–753.

[37] N.J. Petch, The Cleavage Strength of Polycrystals, J. Iron Steel Inst. 174 (1953) 25–28.

[38] R.M. Aikin, The mechanical properties of in-situ composites, JOM. 49 (1997) 35–39. doi:10.1007/BF02914400.

[39] H. Ohtani, S. Okaguchi, Y. Fujishiro, Y. Ohmori, Morphology and properties of low-carbon bainite, Metall. Trans. A. 21 (1990) 877–888. doi:10.1007/BF02656571.

[40] P. Krakhmalev, I. Yadroitsev, Microstructure and properties of intermetallic composite coatings fabricated by selective laser melting of Ti-SiC powder mixtures, Intermetallics.

46 (2014) 147–155. doi:10.1016/j.intermet.2013.11.012.

[41]   T.G.G. Santos, P. Vilaa, R.M.M. Miranda, P. Vilaça, R.M.M. Miranda, Electrical
conductivity field analysis for evaluation of FSW joints in AA6013 and AA7075 alloys, J.
Mater. Process. Technol. 211 (2011) 174–180. doi:10.1016/j.jmatprotec.2010.08.030.